ACS OMEGA

Open Access

http://pubs.acs.org/journal/acsodf

Article

Synthesis and Performance Evaluation of Multialkylated Aromatic Amide Oligomeric Surfactants as Corrosion Inhibitor/Drag Reducing Agents for Natural Gas Pipeline

Feng Li, Bo Yao, Chuanxian Li, Guangyu Sun, Fei Yang,* Hongbo Zeng, and Xinyuan Li

Cite This: *ACS Omega* 2024, 9, 43977−43985

Read Online

ACCESS | Metrics & More | Article Recommendations

ABSTRACT: Drag reducing agents (DRAs) including amphiphiles and polymers can enhance energy efficiency and transmission volume in natural gas pipelines. However, the correlation between DRA molecular structure and drag reduction efficiency remains unclear. In this paper, the multialkylated aromatic amides (MAA) oligomeric surfactants with different numbers of amide group/*n*-dodecane chain (from 1 to 3) were first synthesized and characterized. Then, the potential efficiency of MAA as the corrosion inhibitors (CIs)/DRAs for natural gas pipelines was investigated by interfacial activity analysis, film-forming property test, electrochemical polarization curve measurement, and in-door loop test. The results showed that the molecular structure is the key factor influencing the performance of MAA. By increasing the number of amide group/*n*-dodecane chains, the interfacial activity of MAA improves greatly, thus outstandingly affecting the film-forming property of the MAA on the carbon steel sheet. For MAA-1, the formed film is too thin to cover the surface roughness, and then the corrosion inhibiting (78.64%)/drag reducing (0−2%) rates are the lowest. For MAA-3, the formed film is the thickest and smooth, thus imparting the largest corrosion inhibiting (93.88%)/drag reducing (10−14%) rates to MAA-3. For MAA-2, the formed film is thicker but not smooth, and the corrosion inhibiting (89.88%)/drag reducing (4−6%) rates are intermediate. We speculate that the structure of the MAA greatly influences the adsorption and self-assembly of MAA on the inner pipe wall and then generates different performances. This work is helpful for guiding the development of natural gas DRAs with high efficiency.

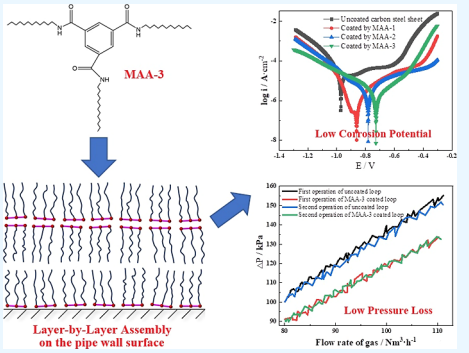

1. INTRODUCTION

Natural gas is a kind of clean energy, and the application of natural gas can reduce the use of coals and oils, thus remarkably alleviating the environmental polluting problem. China's demand for natural gas is increasing rapidly, and new natural gas pipelines are still under development.[1] Gas compressor stations are constructed along the natural gas pipelines and provide pressure energy for the natural gas to overcome the frictional resistance and maintain the gas transmission volume. Natural gas itself has very low viscosity, but under the condition of long distance and high transmission volume, the energy consumption during pipelining is very large. Meanwhile, the demand for natural gas of different regions varies greatly in different seasons, which requires gas pipelines to have a certain degree of transmission flexibility, especially to rapidly increase the transmission volume for guaranteeing the gas supply. Therefore, it is necessary to take technical measures to save energy or increase the transmission volume of gas pipelines.

Two techniques have been practically applied in natural gas pipelines to reduce the friction loss or increase the transmission volume, i.e., the internal coating[2,3] and drag reducing agents (DRAs).[4,5] The flow state of most of the natural gas pipelines is within the resistance square region of turbulent flow, and the hydraulic friction factor λ could be calculated by the Shifrinson equation[6]

$$\lambda = 0.111\left(\frac{K}{D}\right)^{0.25} \tag{1}$$

where K is the surface roughness of pipelines and D is the inner diameter of pipelines. Obviously, the λ is only related to the value of K.[6] By constructing an internal coating such as epoxy coating, the K of the pipelines is outstandingly decreased to several micrometers and then the value of λ decreases, thus reducing the hydraulic friction loss h_f according to the Darcy−Weisbach equation[7] shown below

Received: September 12, 2024
Revised: September 29, 2024
Accepted: October 9, 2024
Published: October 17, 2024

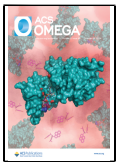

$$h_f = \lambda \frac{L}{D} \frac{V^2}{2g} \quad (2)$$

where L is the pipeline length, V is the flow speed of fluid, and g is the gravitational acceleration. However, the internal coating technique only fits for new pipelines with diameters larger than 500 mm considering the economics. For the gas pipelines in service and the pipelines having small diameters/low pressures, the internal coating is generally not applied.

In comparison, the DRA technique has lower construction cost and wider scope of application, which could be used in both new gas pipelines and service gas pipelines with no diameter/pressure limitations.[4−6] DRAs, which are derived from corrosion inhibitors (CIs), are small molecular or polymeric amphiphiles containing both polar groups and long alkyl chains. MD simulations about the polar groups−iron interaction showed that amine/amide groups have the strongest interaction energy with iron.[8] Therefore, most of the developed DRAs contain amine/amide groups and could be classified into four types: fatty amines, fatty acids, imidazolines, and amides. Two different drag reducing mechanisms of DRAs have been put forward:[9−12] on the one hand, DRA film reduces the surface roughness of the pipelines, thus playing a smooth drag reducing role; on the other hand, some researchers stated that the elastic DRA film also plays an elastic drag reducing role. The DRAs are often dissolved in a volatile solvent (such as ethanol) to prepare the DRA solutions, then the solutions are injected into the natural gas pipelines through atomizing injection or double pipeline pig injection.[13]

Since 1990s, some test loops have been designed and constructed to evaluate the performance of DRAs in the laboratory.[14] The test loops were often equipped with an atomizing injection system to inject the DRAs solution into the loops. Alternatively, the DRA film could also be formed by an immersion film-forming method, that is, filling the test pipe section of the loops with DRA solution to form the DRA film. Field tests of the DRAs have also been carried out in some natural gas pipelines. Overseas, Lowther[15] first applied the DRAs to the natural gas pipelines and achieved the preliminary drag reducing efficiency in field tests. Li et al.[16] evaluated many types of possible DRAs through a self-designed test loop in laboratory and then applied the selected Nalco945 CI to an offshore dry gas pipeline in Mexico for drag reducing purpose. After that, Chen et al.[17] successfully carried out the field tests by using specific CIs as the DRAs in a natural gas pipeline of Mexico bay. Naess[12] classified the DRAs into two types, film-forming agents and viscoelastic agents, and the performance and drag reducing mechanism of the two type DRAs were well studied based on an in-door test loop. In China, Xing[18] synthesized three DRAs including stearic imidazole, AAMT, and VI-VTMS copolymers and evaluated the three DRAs based on a self-developed test loop. It was found that the drag reducing efficiency of the three DRAs was 8.4% for stearic imidazole, 10% for AAMT, and 22.7% for the copolymers. Bao et al.[19] synthesized BIB DRAs and evaluated it through the in-door loop tests and field tests. In the field tests, the BIB DRAs were injected into the pipelines by atomizing injection, and the drag reducing efficiency and drag reducing duration were 8−10% and 90 d, respectively. Xu et al.[20] evaluated the performance of a polymer-type DRA both in No. 1 oil production plant of Changqing oilfield and in a long-distance natural gas pipeline from Lanzhou to Yinchuan. It was found that the drag reducing efficiency is 19.5% in the oilfield but 10% in the gas pipeline. Ma[21] et al. prepared the CPA DRAs and applied it in the Shanxi-Beijing natural gas pipeline, and the field test showed that the maximum drag reducing rate of CPA could achieve 25%.

Although much work has been carried out on the DRAs as mentioned above, the effect of the molecular structure of DRAs on their performance is still unclear. Oligomeric surfactants are composed by two or more monomer surfactants of the same type, which are chemically bonded together by small linkers (such as methyl) at or near the hydrophilic headgroup.[22,23] Obviously, oligomeric surfactants have multiple polar groups and nonpolar long alkyl chains, which imparts them high surface activity, low critical micellar concentration, and versatile self-assemble structures.[22,23] The superior properties of oligomeric surfactants look promising in different applications.[22,23] Some studies have also shown that the different positions of heteroatoms or functional groups on oligomeric surfactants have a significant impact on their stability, physical and chemical properties, chemical reactivity, and coordination bonds. This affects their ability to establish stable coordination interactions with metal surfaces, thereby affecting their corrosion inhibition effect.[24,25] In a former published paper,[26] we synthesized a series of multialkylated aromatic amide (MAA) oligomeric surfactant containing different number of amide group/*n*-dodecane chain (1−3) and evaluated the performance of MAA as asphaltene dispersant. It was found that the performance of MAA improved by increasing the number of amide group/*n*-dodecane chain, and MAA-3 showed the best performance.

In existing research,[27−30] various CIs with different structures and properties have been synthesized, and their effects mainly focus on their adsorption capacity on metal surfaces and corrosion resistance. However, there is relatively little research on their drag reduction performance for natural gas pipelines. Therefore, in this work, the potential efficiency of MAA as the CIs/DRAs for natural gas pipelines was investigated by interfacial activity analysis, film-forming property test, electrochemical polarization curve measurement, and in-door loop test. The results showed that the corrosion inhibiting/drag reducing efficiency is closely related to the molecular structure of MAA. With the increase of the number of amide group/*n*-dodecane chain (from 1 to 3), the MAA showed much stronger interfacial activity and film-forming property, thus imparting better CIs/DRA performance to the MAA.

2. EXPERIMENTAL SECTION

2.1. Materials. The water used here was double distillated water. The chemicals including HCl, NaOH, petroleum ether, toluene, ethanol, and acetone were purchased from Tianjin Fuyu Fine Chemical Co. Other chemicals such as methyl benzoate, dimethyl phthalate, trimethyl homophthalate, and dodecylamine were purchased from Shanghai Aladdin Biochemical Technology Co. All of the above reagents were of analytical grade and were used as received. The carbon steel sheets used in film-forming tests and electrochemical polarization curve measurements were purchased from the Chinese Yangzhou Xiangwei Machinery Co. The size of the carbon steel sheets is 50 mm*25 mm.

2.2. Synthesis of the MAA Oligomeric Surfactant. The methyl benzoate, dimethyl phthalate, and trimethyl homophthalate were amidated with dodecylamine (the molar ratio of

https://doi.org/10.1021/acsomega.4c08381
ACS Omega 2024, 9, 43977−43985

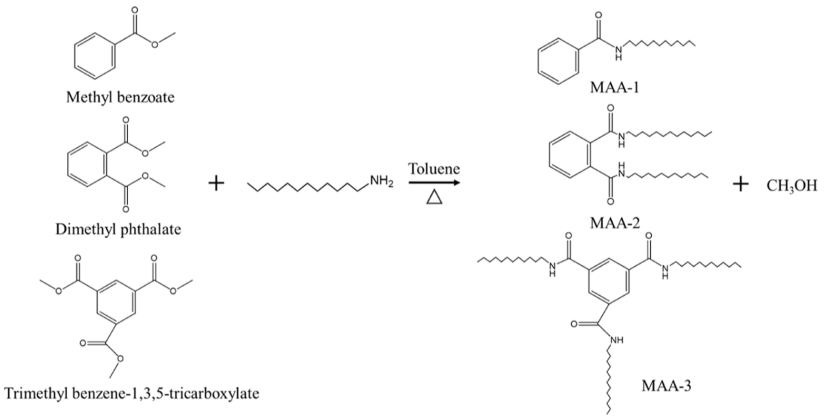

Figure 1. Synthesis process of the MAA oligomeric surfactant.

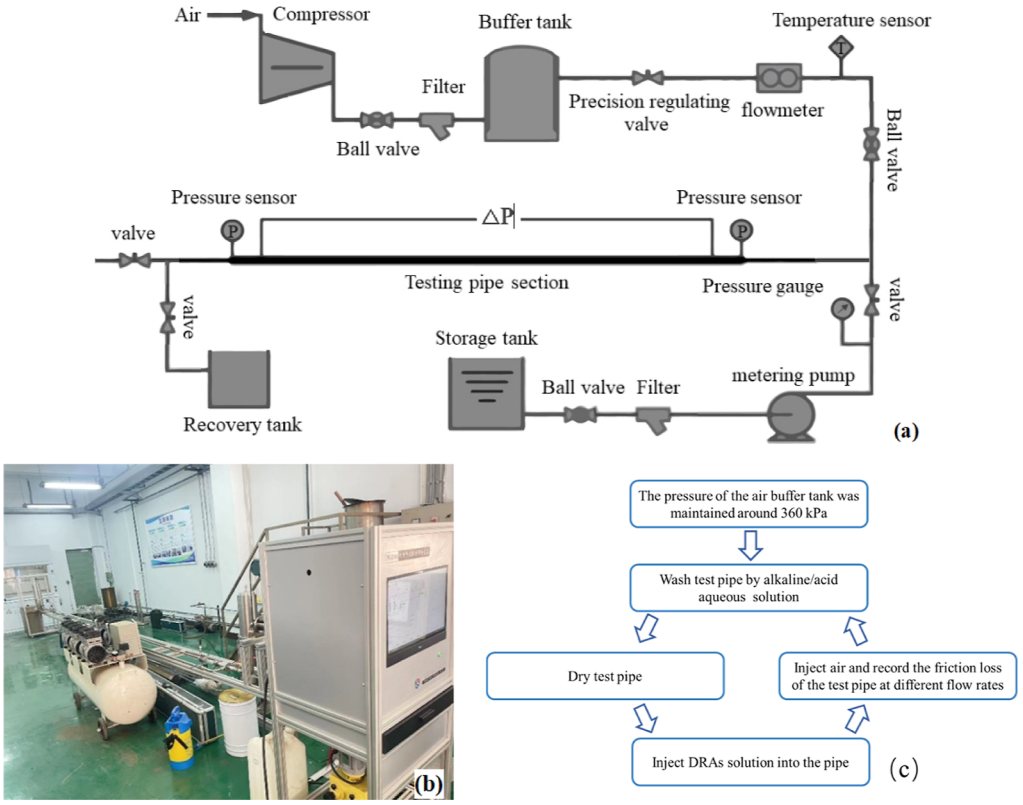

Figure 2. Schematic diagram (a), physical picture (b), and experimental procedure (c) of the in-door test loop.

the ester group to amino group was fixed at 1:1.05) to obtain the MAA oligomeric surfactant. Toluene was used as the solvent, and the reaction temperature and reaction time were set at 130 °C and 12 h, respectively. After reaction, the toluene solvent was evaporated by vacuum distillation, and the obtained solid products were washed by HCl aqueous solution to remove excess dodecylamine. After that, the products were dried in a vacuum oven to obtain MAA-1, MAA-2, and MAA-3. Figure 1 demonstrates the reacting routes and the molecular structure of the products. The density of MAA measured by the specific gravity bottle method is 0.866 g/cm^3 for MAA-1, 0.911 g/cm^3 for MAA-2, and 0.972 g/cm^3 for MAA-3. The MAA is easy to dissolve in ethanol and toluene but cannot be dissolved in water. The MAA-ethanol solutions with the MAA concentration less than 50 g·L^{-1} are transparent liquid at room temperature. Therefore, ethanol was selected as the solvent of MAA, and the concentration of MAA in the solutions was fixed at 1, 2, 5, 10, and 20 g·L^{-1}.

2.3. Methods. *2.3.1. Structural Characterization of the MAA.* The Nicolet IS50 Fourier transform infrared spectrometer produced by Thermo Fisher Scientific of America was used for structural determination of MAA. The spectrometer was pretreated and preheated for 40 min before spectral measurement. The KBr pressing method was used, the ambient temperature was 25 °C, and the ambient humidity was 50%.

2.3.2. Interfacial Activity Tests of the MAA. MAA-1, MAA-2, and MAA-3 were dissolved in toluene at different concentrations, and then the MAA-toluene solution/water interfacial tension was measured by the Tracker interfacial rheometer produced by TECLIS company of France: in the water environment, a drop of MAA-toluene solution was squeezed out by a syringe under a certain pressure difference

https://doi.org/10.1021/acsomega.4c08381
ACS Omega 2024, 9, 43977−43985

(ΔP), then the shape of the solution drop was photographed and analyzed by Laplace's equation to obtain the MAA-toluene solution/water interfacial tension.[31,32] Each sample is tested three times to ensure the accuracy of the results.

2.3.3. Film-Forming Analysis of the MAA. Pretreatment of carbon steel sheets: first, the sheets were rinsed by petroleum ether and dried with absorbent paper; then the sheets were polished by the abrasive paper grit 800−1200; after polishing, the sheets were washed with ethanol, acetone, and water in turn and dried, and the mass of each sheet was recorded as m_1. The treated sheets were immersed in bottles containing different concentrations of MAA solutions for film formation experiments. After film formation for a certain time, the sheets were taken out and dried by absorbent paper, and the mass of each sheet after MAA adsorption was recorded as m_2. By comparing the mass changes of carbon steel sheets before and after immersion, the thickness of the MAA film (THK) adsorbed on the sheet surface can be calculated as follows

$$\mathrm{THK} = \frac{m_1 - m_2}{\rho S} \tag{3}$$

where S is the surface area of steel sheet; ρ is the density of the MAA. Each sample was tested three times to ensure the accuracy of the results.

The surface roughness of the carbon steel sheets before/after MAA adsorption was investigated by NApreos field emission SEM (Thermo Fisher Scientific, America).

2.3.4. Corrosion Inhibiting Analysis of the MAA. The corrosion inhibiting performance of the MAA was studied by measuring the electrochemical polarization curves of the uncoated carbon steel sheets and the sheets coated by the MAA film. A CHI604E electrochemical workstation (Shanghai Chenhua Instrument Co., China) fitted with three-electrode system was used here: the auxiliary electrode is the platinum electrode, the reference electrode is the saturated calomel electrode, and the working electrode is the carbon steel sheet uncoated/coated by DRAs film. The potential scanning range is −1.5−0 V, and the scanning rate is 0.5 $\mathrm{mV{\cdot}s^{-1}}$. The corrosion inhibiting rate CI of the MAA can be calculated as follows

$$CI = \frac{i_{\mathrm{corr1}} - i_{\mathrm{corr2}}}{i_{\mathrm{corr1}}} \times 100\% \tag{4}$$

where i_{corr1} is the corrosion current density of the uncoated carbon steel sheet; i_{corr2} is the corrosion current density of the carbon steel sheet coated by MAA film.

2.3.5. Drag Reducing Evaluation of the MAA by the In-Door Test Loop. An in-door test loop system was designed and established for the drag reducing evaluation of DRAs. The schematic diagram and physical picture of the test loop are demonstrated in Figure 2a,b. As seen in the figure, the loop contains a gas compressor, a gas flowmeter, a liquid pump, a carbon steel testing pipe section, an air buffer tank, a recovery tank, pressure sensors, temperature sensor, filters, and valves. The pressure of the air buffer tank was maintained at around 360 kPa by the gas compressor. The inner diameter and length of the testing pipe section are 12 mm and 6 m, respectively. In order to guarantee that the flow state of the air in the testing pipe is within the resistance square region, the Reynolds number (Re) of the air flow in the testing pipe should be larger than the second boundary Reynolds number (Re_2)[33]

$$\mathrm{Re} = \frac{4Q\rho}{\pi D\mu} > \mathrm{Re}_2 = 11\left(\frac{D}{K}\right)^{1.5} \tag{5}$$

where Q is the flow rate, μ is the dynamic viscosity of air, ρ is the density of air. Imaging the roughness of the testing pipe as the limit small value 10 μm and the viscosity of the air at 25 °C as 1.81×10^{-5} Pa·s,[17] the flow rate should be larger than 80 $\mathrm{m^3/h}$ to maintain the flow state of air in the resistance square region.

The experimental procedure diagram is shown in Figure 2c. The testing pipe section is detachable, and before carrying out drag reducing tests, the detached test pipe was washed by alkaline/acid aqueous solution, water, and ethanal to clean up the testing pipe; then, the testing pipe was dried and installed into the loop system; after that, the DRA solution was injected into the testing pipe by pump and the MAA film was formed on the testing pipe by the immersion film-forming method; finally, the friction loss (ΔP) of the testing pipe under different flow rates was recorded by the data acquisition system. The drag reducing rate DR of the MAA could be calculated as follows

$$\mathrm{DR} = \frac{\Delta P_1 - \Delta P_2}{\Delta P_1} \times 100\% \tag{6}$$

where ΔP_1 is the friction loss of the uncoated testing pipe, ΔP_2 is the friction loss of the testing pipe coated by MAA film. After each experiment, the testing pipe coated with MAA was cleaned and dried for the next experiment.

3. RESULTS AND DISCUSSION

3.1. Structural Characterization of the MAA. Taking MAA-1 as an example, the FT-IR curves of the methyl benzoate and MAA-1 are shown in Figure 3. The methyl benzoate contains ester group, and the feature peaks of C═O, C−O−C antisymmetric, and symmetric stretching vibrations are obviously seen at 1796, 1279, and 1112 $\mathrm{cm^{-1}}$. For MAA-1, the ester group is replaced by the amide group. The N−H, C═O and C−N feature peaks of the amide group appeared near 3329, 1635, and 1240 $\mathrm{cm^{-1}}$, respectively. Meanwhile, the C−O−C peaks disappear in the FT-IR curve of MAA-1. It could be concluded that MAA is successfully synthesized.

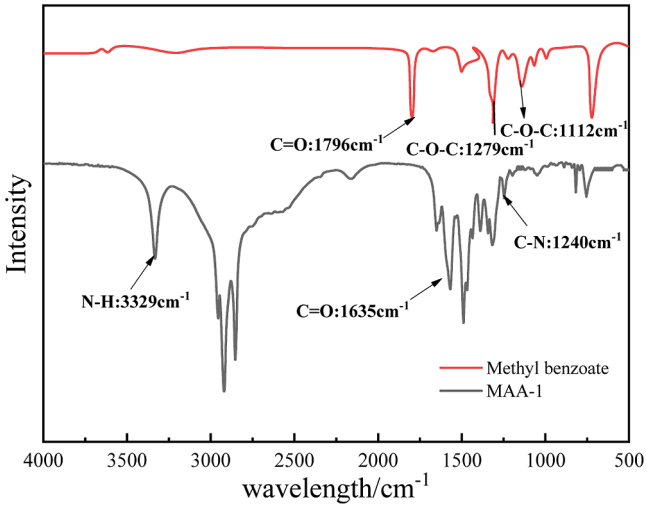

Figure 3. FI-IR curves of the methyl benzoate and MAA-1.

https://doi.org/10.1021/acsomega.4c08381
ACS Omega 2024, 9, 43977−43985

3.2. Interfacial Activity of the MAA. The effect of MAA on the toluene/water interfacial tension is described in Figure 4. Obviously, increasing the number of the amide group/*n*-dodecane chain greatly enhances the interfacial activity of MAA, and the sequence of the interfacial activity of MAA is MAA-3 > MAA-2 > MAA-1. For example, at the fixed concentration of 100 ppm, adding MAA-1 only slightly decreases the interfacial tension from the initial 34.55 mN·m^{-1} to 34.06 mN·m^{-1}, while MAA-2 and MAA-3 decrease the interfacial tension to 27.17 mN·m^{-1} and 15.87 mN·m^{-1}, respectively. The interfacial tension also decreases with an increase in the MAA concentration, indicating that more MAA molecules adsorb on the toluene/water interface. The interfacial tension reducing trend of MAA-3 with increasing concentration is the most outstanding. At the MAA-3 concentration of 1000 ppm, the interfacial tension could not be measured due to the unstable MAA-toluene solution drop in the water phase.

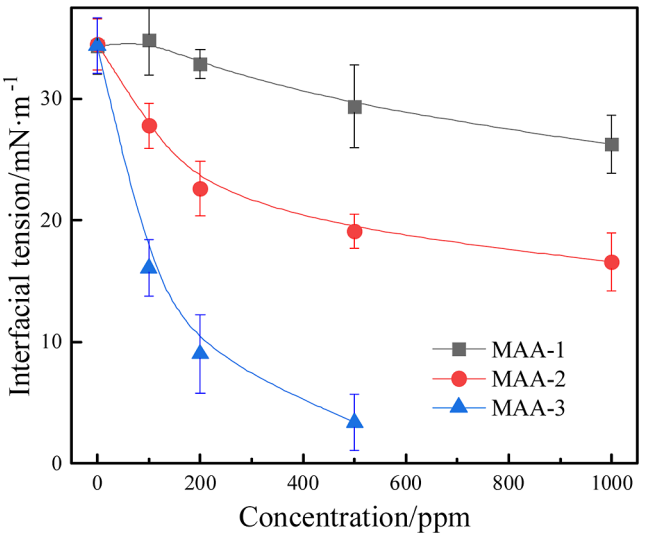

Figure 4. Effect of the MAA concentration on the toluene/water interfacial tension.

3.3. Film-Forming Properties of the MAA. At a fixed film forming time of 3 h, the effect of MAA concentration on the thickness of the film formed on the carbon steel sheet surface is shown in Figure 5a. The film thickness increases with increasing the MAA concentration. We consider that the MAA adsorbs on the carbon steel sheet and forms multilayer film. Increasing the MAA concentration facilitates the MAA adsorption and then increases the film thickness. Increasing the number of the amide group/*n*-dodecane chain also facilitates the MAA adsorption. For MAA-1, the film thickness increases from 0.04 μm at 1 g·L^{-1} to 1.12 μm at 20 g·L^{-1}; for MAA-2, the film thickness increases from 0.23 μm at 1 g·L^{-1} to 3.48 μm at 20 g·L^{-1}; and for MAA-3, the film thickness increases from 0.45 μm at 1 g·L^{-1} to 4.11 μm at 20 g·L^{-1}. The results are in accordance with the interfacial activity of the MAA.

At the fixed MAA concentration of 20 g·L^{-1}, the film thickness first increases quickly with increasing film forming time. At the film forming time larger than 6 h, the film thickness increasing rate becomes very slow. Therefore, the film forming time was fixed at 6 h in the latter work, at which the film thickness of MAA-1, MAA-2, and MAA-3 is 1.33, 3.75, and 4.35 μm, respectively.

Figure 6 shows the microscopic morphology of the carbon steel sheets uncoated/coated by MAA. As seen in Figure 6a, the surface of the uncoated sheet has horizontal striped veins, which is possibly produced by the abrasive paper polishing.

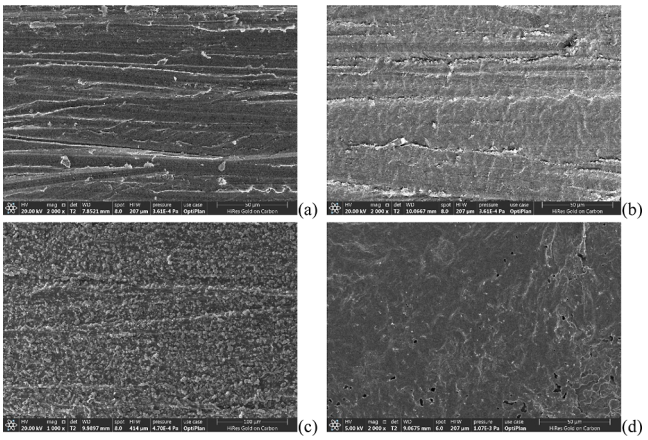

Figure 6. SEM images of the carbon steel sheets: (a) uncoated; (b) coated by MAA-1; (c) coated by MAA-2; and (d) coated by MAA-3. The film forming time and MAA concentration were fixed at 6 h and 20 g·L^{-1}, respectively.

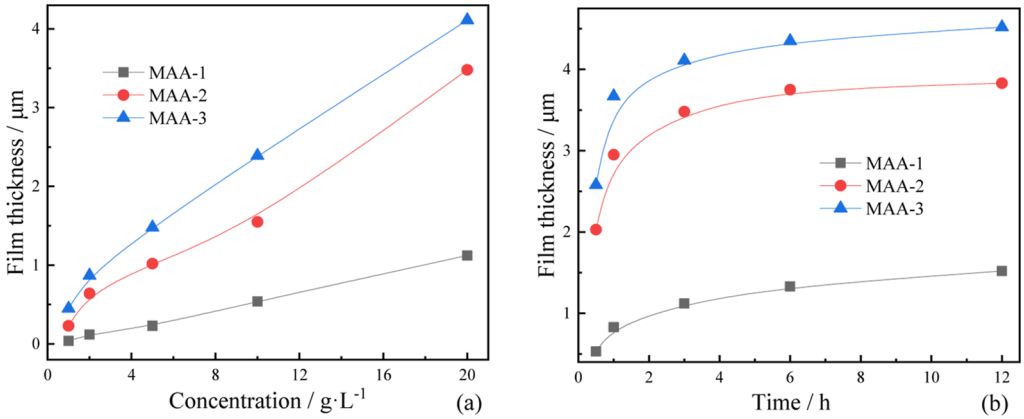

Figure 5. Effect of MAA concentration on the film thickness at the fixed film forming time 3 h (a); effect of film forming time on the film thickness at the fixed MAA concentration 20 g·L^{-1} (b).

https://doi.org/10.1021/acsomega.4c08381
ACS Omega 2024, 9, 43977−43985

The roughness of the surface is about several μm based the scale bar of the figure (50 μm). For the sheet coated by MAA-1 (see Figure 6b), the surface roughness decreases to some extent but still has horizontal striped veins, indicating that the MAA-1 film is very thin and could not effectively cover the surface roughness of the sheet. As seen in Figure 6c, the MAA-2 film covers the surface roughness of the sheet and we could not find clear horizontal veins. However, the MAA-2 film is not smooth. The adsorption of MAA-3 on the sheet generates a complete and smooth film (see Figure 6d), which favors the drag reduction of the natural gas pipelines. The MAA-3 has the strongest interfacial activity (see Figure 4), and then the formed MAA-3 film should be thicker and more compact, which is beneficial for the formation of a complete and smooth film.

3.4. Corrosion Inhibiting Efficiency of the MAA. The electrochemical polarization curves of the carbon steel sheet uncoated/coated by the MAA film can be seen in Figure 7.

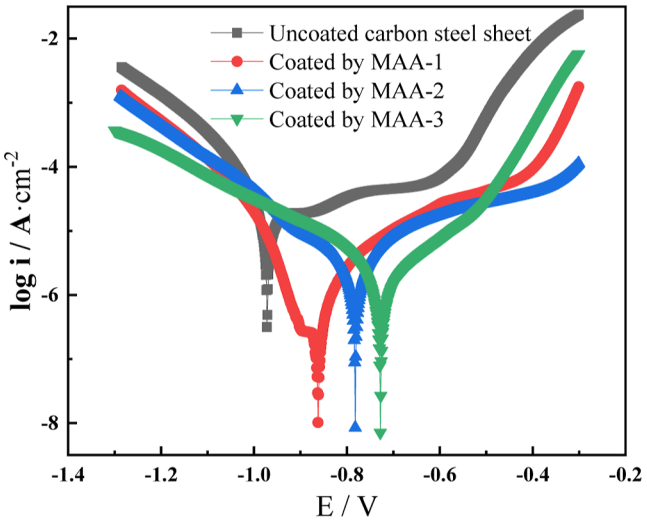

Figure 7. Electrochemical polarization curves of the carbon steel sheet uncoated/coated by MAA films. The film forming time and MAA concentration were fixed at 6 h and 20 g·L^{-1}, respectively.

Each experiment was tested twice, and the experimental result curves basically overlapped. Compared with the polarization curve of uncoated carbon steel sheet, the polarization curves of coated sheets change outstandingly: the corrosion potential E moves toward the positive direction, which indicates that the MAA belongs to the anodic type of CIs. Based on Figure 7, the corrosion current density i and the corrosion inhibiting rate were calculated and are shown in Table 1. The value of i of the uncoated carbon steel sheet is 35.62 μA·cm^{-2}. After being coated by MAA-1, MAA-2, and MAA-3, the values of i reduce to 7.61, 3.61, and 2.18 μA·cm^{-2}, respectively. The corresponding corrosion inhibiting rates are 78.64%, 89.88%, and 93.88%, successively. It is clear that increasing the number of the amide group/n-dodecane chain greatly reduces the value of i but enhances the corrosion inhibiting rate, which is in accordance with the interfacial activity of the MAA.

Table 1. Values of E, i, and Corrosion Inhibiting Rate of the Carbon Steel Sheet Uncoated/Coated by MAA Film Calculated from Figure 7

carbon steel sheet	E/V	i/μA·cm^{-2}	corrosion inhibiting rate/%
uncoated	−0.972	35.62	/
coated by MAA-1	−0.862	7.61	78.64
coated by MAA-2	−0.781	3.61	89.88
coated by MAA-3	−0.727	2.18	93.88

3.5. Drag Reducing Evaluation of the MAA. Figure 8 shows the friction loss of the testing pipe uncoated (ΔP_1)/coated (ΔP_2) by MAA. Each set of experiments was tested twice to guarantee the reproducibility. As seen in Figure 8a, the values of ΔP_1 and ΔP_2 increase gradually by increasing the flow rate of gas, and ΔP_1 is lightly higher than ΔP_2, indicating that the coated MAA-1 film does show a certain drag reducing ability for the testing pipe. However, the gap between ΔP_1 and ΔP_2 is very small; this indicates that the drag reducing efficiency of the coated MAA-1 film is poor, which is caused by the poor interfacial activity and film-forming properties of MAA-1. With the increase of the gas flow rate, the gap between ΔP_1 and ΔP_2 is widened to some extent, which means increasing the gas flow rate improves the drag reducing efficiency of the coated MAA-1 film. In general, the coated MAA-1 film has poor drag reducing efficiency, and the drag reducing rate calculated by eq 6 is only in the range of 0−2%.

As seen in Figure 8b, the gap between ΔP_1 and ΔP_2 is clearly widened by the coated MAA-2 film, indicating that the coated MAA-2 film has a stronger drag reducing ability than the coated MAA-1 film. Meanwhile, increasing the gas flow rate also slightly widens the gap between ΔP_1 and ΔP_2 and then improves the drag reducing ability of the coated MAA-2 film. Based on eq 6, the drag reducing rate of coated MAA-2 film is in the range of 4−6%.

As seen in Figure 8c, the gap between ΔP_1 and ΔP_2 is the widest for the coated MAA-3 film, and the drag reducing rate of the coated MAA-3 film achieves to 10−14%. The MAA-3 has the strongest interfacial activity and the best film-forming properties, thus imparting MAA-3 film the best drag reducing ability.

3.6. Drag Reducing Mechanism Discussion of the MAA. The thickness and morphology of the MAA film coated on the inner pipe wall have the key influence on the drag reducing ability of MAA. We consider that the thickness and morphology of the MAA film are dominated by the self-assemble behavior of the MAA molecules at the inner pipe wall surface, and the molecular structure of the MAA greatly affects its self-assemble behavior.

As seen in Figure 9a, MAA-1 first adsorbs and lies on the inner pipe wall to form an adsorbed MAA-1 layer. The lying state is induced by the poor interfacial activity of MMA-1. Then, additional MAA-1 molecules continuously assemble on the layer by the $\pi-\pi$ interaction, hydrogen bond and polar attraction, thus forming a film coated on the inner pipe surface. Because of the lying state of MAA-1 molecules, the formed MAA-1 film is very thin and could not effectively smooth the inner pipe surface. Therefore, the drag reducing ability of the MAA-1 is poor.

In comparison, MAA-3 has the strongest interfacial activity, and then the three alkyl chains of the MAA-3 molecules adsorbed on the inner pipe wall are nearly vertical to the pipe wall (see Figure 9b). Then, the second layer of MAA-3 assembles through the interactions of the nonpolar alkyl chains (see Figure 9b). After that, the MAA-3 repeats the process mentioned above and assembles layer by layer. Finally, a thick and smooth MAA-3 film will be formed, which imparts the MAA-3 with the best drag reducing ability.

https://doi.org/10.1021/acsomega.4c08381
ACS Omega 2024, 9, 43977−43985

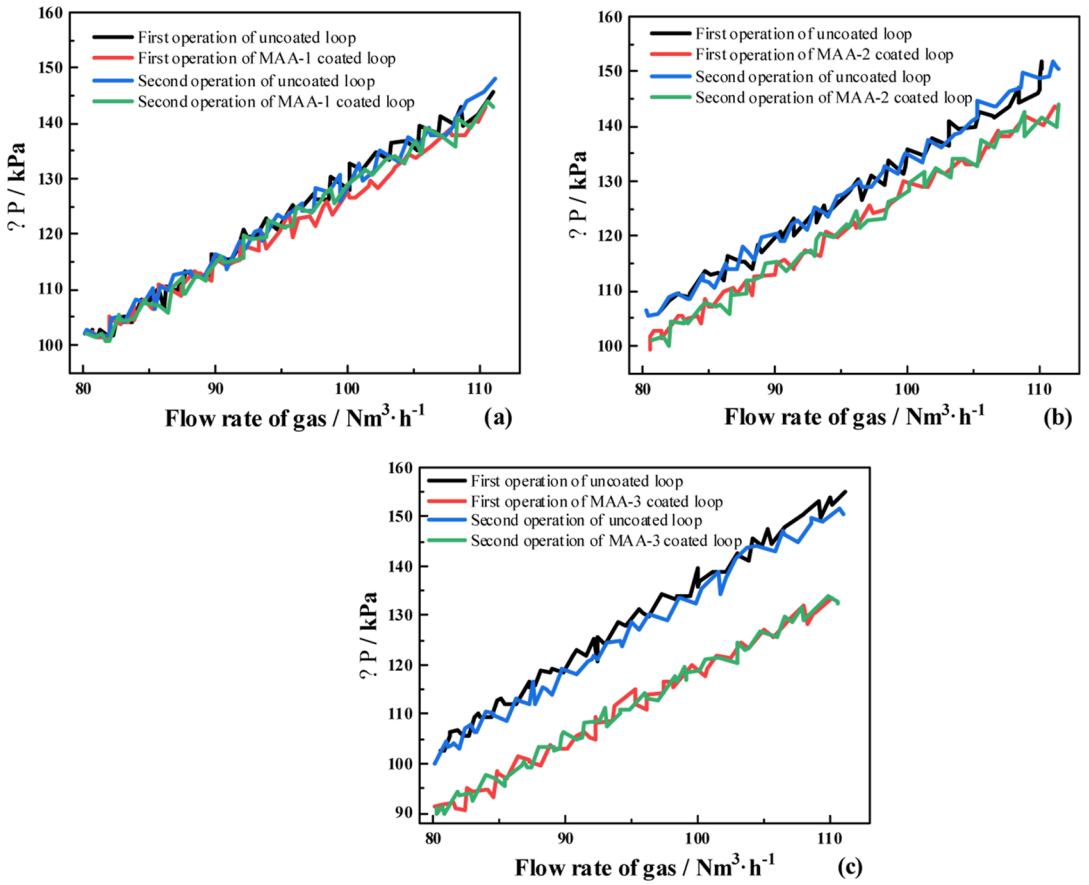

Figure 8. Variation of ΔP of the testing pipe section with flow rate of gas: (a) uncoated/coated by MAA-1; (b) uncoated/coated by MAA-2; and (c) uncoated/coated by MAA-3.

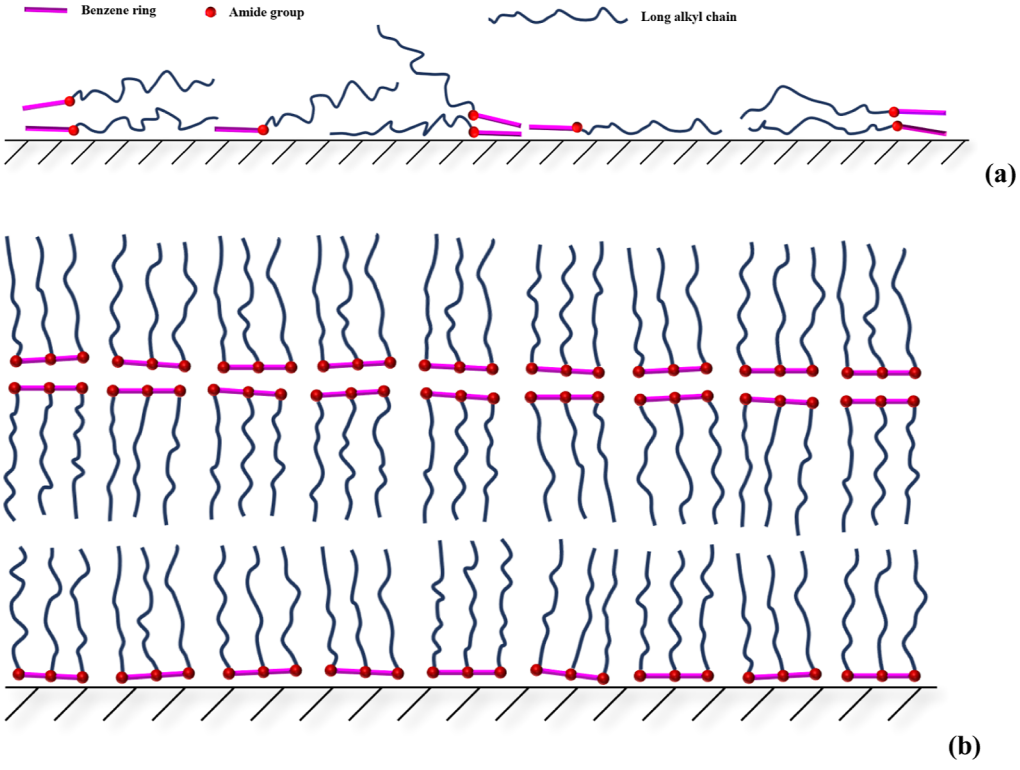

Figure 9. Schematic diagram of the adsorption and self-assembly of MAA molecules on the inner pipe wall: (a) MAA-1 and (b) MAA-3.

https://doi.org/10.1021/acsomega.4c08381
ACS Omega 2024, 9, 43977−43985

The interfacial activity of MAA-2 is intermittent for MAA-1 and MAA-3. Therefore, the formed MAA-2 film is much thicker than the MAA-1 film but thinner than the MAA-3 film. Meanwhile, the MAA-2 molecules could not form an ordered layer-by-layer assembly structure like the MAA-3 molecules. Therefore, the surface of the MAA-2 film is not as smooth as that of the MAA-3 film, which weakens the drag reducing ability of MAA-2.

4. CONCLUSIONS

The MAA oligomeric surfactants with different numbers of amide group/*n*-dodecane chain (from 1 to 3) were successfully synthesized, and the potential efficiency of MAA as the CIs/DRAs for natural gas pipelines was investigated. The conclusions are as follows:

(1) With the increase of the number of amide group/*n*-dodecane chain, the interfacial activity of MAA increases greatly. At the fixed concentration 100 ppm, the toluene/water interfacial tension decreases from the initial 34.55 $mN{\cdot}m^{-1}$ to 34.06 $mN{\cdot}m^{-1}$ for MAA-1, 27.17 $mN{\cdot}m^{-1}$ for MAA-2, and 15.87 $mN{\cdot}m^{-1}$ for MAA-3. Increasing the MAA concentration also outstandingly reduces the interfacial tension.

(2) With the increase of MAA concentration or the film-forming time, the thickness of the MAA film formed on the carbon steel sheet increases continuously. The MAA-1 film is too thin to cover the surface roughness of the sheet, while the MAA-3 film is the thickest and is smooth. Although the MAA-2 film is relatively thick, but the film is not smooth.

(3) The number of amide group/*n*-dodecane chain dominates the performance of MAA. For MAA-1, the corrosion inhibiting rate (78.64%) and drag reducing rate (0−2%) are the lowest. For MAA-3, the formed film has the largest corrosion inhibiting rate (93.88%) and drag reducing rate (10−14%). For MAA-2, the corrosion inhibiting rate (89.88%) and drag reducing rate (4−6%) are intermediate. We speculate that the structure of the MAA greatly influences the adsorption and self-assembly of MAA on the inner pipe wall and then generates different performances.

AUTHOR INFORMATION

Corresponding Author

Fei Yang − *College of Pipeline and Civil Engineering, China University of Petroleum, Qingdao, Shandong 266580, PR China;* orcid.org/0000-0002-0705-0006; Email: yf9712220@sina.com

Authors

Feng Li − *CNOOC Gas & Power Group, Beijing 100028, PR China*

Bo Yao − *College of Pipeline and Civil Engineering, China University of Petroleum, Qingdao, Shandong 266580, PR China;* orcid.org/0000-0001-8029-2514

Chuanxian Li − *College of Pipeline and Civil Engineering, China University of Petroleum, Qingdao, Shandong 266580, PR China;* orcid.org/0000-0002-2133-6676

Guangyu Sun − *College of Pipeline and Civil Engineering, China University of Petroleum, Qingdao, Shandong 266580, PR China;* orcid.org/0000-0002-3598-3807

Hongbo Zeng − *Department of Chemical and Materials Engineering, University of Alberta, Edmonton, AB T6G 1H9, Canada;* orcid.org/0000-0002-1432-5979

Xinyuan Li − *Sino Oil King Shine Chemical Co., Ltd, Langfang, Hebei 065000, PR China*

Complete contact information is available at: https://pubs.acs.org/10.1021/acsomega.4c08381

Notes

The authors declare no competing financial interest.

ACKNOWLEDGMENTS

Support from the National Natural Science Foundation of China (Grant no. 51774311) is gratefully acknowledged.

REFERENCES

(1) Wang, Y.; Chen, X.; Ren, S. Clean energy adoption and maternal health: Evidence from China. *Energy Econ.* **2019**, *84*, 104517.

(2) Yang, X. H.; Zhu, W. L.; Lin, Z.; Huo, J. J. Aerodynamic evaluation of an internal epoxy coating in nature gas pipeline. *Prog. Org. Coat.* **2005**, *54* (1), 73−77.

(3) Taghavi, N. Economic investigation on the use of internal coating for natural gas trunk-lines. *Chem. Eng. Res. Des.* **2013**, *91* (9), 1725−1730.

(4) Luo, Y.; Liu, Y.; Zhang, D. Y. Advanced progresses in nature gas pipelining applying different drag reduction/energy saving technologies: A review. *Eur. J. Environ. Civ. Eng.* **2015**, *19* (8), 931−949.

(5) Okyere, M. S.; Damoah, L. N. W.; Nyankson, E.; Konadu, D. S. Synergetic Effect of a Drag Reducer and Pipeline Internal Coating on Capacity Enhancement in Oil and Gas Pipelines: a Literature Review. *Eur. J. Mater. Sci. Eng.* **2022**, *7* (2), 75−93.

(6) Huang, Z.; Chen, Z.; Li, Q.; Zhu, R.; Jing, S.; Zhou, Y.; Ma, Y.; Wang, N.; Chang, W. Experimental research on the drag reduction mechanism of natural gas drag reduction agent and its industrial field test. *Ind. Eng. Chem. Res.* **2014**, *53* (31), 12494−12501.

(7) Samadianfard, S. Gene expression programming analysis of implicit Colebrook−White equation in turbulent flow friction factor calculation. *J. Pet. Sci. Eng.* **2012**, *92*−*93*, 48−55.

(8) Li, G., Zhang, Z., Liu, B., Li, C., Chang, W., Bao, X.. Study on Natural Gas Drag Reduction Agent and Mechanism of Gas Pipelines Drag Reduction. In *International Pipeline Conference*, **2008**, Vol. *48609*: pp 113−124, .

(9) Olivares-Xometl, O.; Likhanova, N. V.; Domínguez-Aguilar, M. A.; et al. Surface analysis of inhibitor films formed by imidazolines and amides on mild steel in an acidic environment. *Appl. Surf. Sci.* **2006**, *252* (6), 2139−2152.

(10) Li, F.; Xing, W. G.; Zhang, J.; et al. Drag reduction performance of a combinational natural gas drag reduction agent (DRA) based on mercapto-triazole compound. *Nat. Gas Ind.* **2010**, *30* (11), 87−91.

(11) Ma, Y.; Huang, Z.; Lian, Z.; Chang, W.; Tan, H. Effects of a new drag reduction agent on natural gas pipeline transportation. *Adv. Mech. Eng.* **2019**, *11* (10), 1687814019881923.

(12) Naess, R. Drag Reduction Agents for Natural Gas Flow in Pipelines, Department of Petroleum Engineering and Applied Geophysics of NTNU, Norway, 1999.

(13) Yi, X., Jing, J., Fan, Z., et al. Research Progress of Natural Gas Pipeline Drag Reducing Agents. In *Proceedings of the 2018 National Natural Gas Academic Annual Conference (05 Storage and Pipeline Transportation)*, 2018: pp 229−248. (in Chinese).

(14) Chen, J.; Zhao, W.; Di, Y.; Jia, B.; Wang, J.; Li, H. Apparatus for Testing Drag Reducing Agents in Gas Transmission Pipelines; In *International Pipeline Conference*; American Society of Mechanical Engineers, 2016; Vol. *50275*, p V003T04A036..

(15) Lowther, F. E. Drag reduction method for gas pipelines. US5020561A, 1990.

(16) Li, Y. H.; Chesnut, G. R.; Richmond, R. D.; Beer, G. L.; Caldarera, V. P. Laboratory tests and field implementation of gas-drag-reduction chemicals. *SPE Prod. Facil.* **1998**, *13* (01), 53−58.
(17) Chen, H. J.; Kouba, G. E.; Fouchi, M. S.; et al. Field application of a drag reducing agent to increase gas production. In *NACE CORROSION, NACE-00073*; NACE, 2000.
(18) Xing, W. Development of natural gas DRAs and studying on the drag reducing performance, School of Chemistry and Chemical Engineering of Shandong University, China, 2010 (in Chinese).
(19) Bao, X.; Zhang, J.; Zhang, X.; et al. Synthesis and application of BIB natural gas DRA. *Oil Gas Storage Transp.* **2010**, *29* (2), 113−117. (in Chinese)
(20) Xu, H.; Gao, Y.; Li, G.; Zhang, Z.; Chang, W. Synthesis, Performance Evaluation and Field Application of Polymer-Type Natural Gas Drag Reduction Agent. In *International Pipeline Conference*; American Society of Mechanical Engineers, 2012, pp 515−521..*45127*
(21) Ma, Y.; Huang, Z.; Lian, Z.; Chang, W.; Tan, H. Effects of a new drag reduction agent on natural gas pipeline transportation. *Adv. Mech. Eng.* **2019**, *11* (10), 1−12.
(22) Zana, R. Dimeric and oligomeric surfactants. Behavior at interfaces and in aqueous solution: a review. *Adv. Colloid Interface Sci.* **2002**, *97* (1−3), 205−253.
(23) Fan, Y.; Wang, Y. Self-assembly and functions of star-shaped oligomeric surfactants. *Langmuir* **2018**, *34* (38), 11220−11241.
(24) Verma, C.; Alfantazi, A.; Quraishi, M. A.; Rhee, K. Y. Significance of Hammett and Taft substituent constants on bonding potential of organic corrosion inhibitors: Tailoring of reactivity and performance. *Coord. Chem. Rev.* **2023**, *495*, 215385.
(25) Verma, C.; Singh, A.; Singh, P.; Yop Rhee, K.; Alfantazi, A. Regioisomeric effect of heteroatoms and functional groups of organic ligands: Impacts on coordination bonding and corrosion protection performance. *Coord. Chem. Rev.* **2024**, *515*, 215966.
(26) Yang, F.; Duan, Z.; Liu, D.; Li, C.; Sun, G.; Zhang, H.; Yao, B. Multi-alkylated aromatic amides amphiphiles effectively stabilize the associated asphaltene particles in crude oil. *J. Pet. Sci. Eng.* **2022**, *212*, 110204.
(27) Jafari, H.; Akbarzade, K.; Danaee, I. Corrosion inhibition of carbon steel immersed in a 1M HCl solution using benzothiazole derivatives. *Arab. J. Chem.* **2019**, *12* (7), 1387−1394.
(28) Jafari, H.; Ameri, E.; Vakili, M. H.; Berisha, A. Novel Silicon-based schiff-base as corrosion inhibitor for anti-corrosion behavior of API 5L Grade B in 1M HCl. *Mater. Chem. Phys.* **2024**, *311*, 128499.
(29) Jafari, H.; Danaee, I.; Eskandari, H.; RashvandAvei, M. Combined Computational and Experimental Study on the Adsorption and Inhibition Effects of N2O2 Schiff Base on the Corrosion of API 5L Grade B Steel in 1 mol/L HCl. *J. Mater. Sci. Technol.* **2014**, *30* (3), 239−252.
(30) Jafari, H.; Ameri, E.; Rezaeivala, M.; Berisha, A.; Halili, J. Anti-corrosion behavior of two N2O4 Schiff-base ligands: Experimental and theoretical studies. *J. Phys. Chem. Solids* **2022**, *164*, 110645.
(31) Liu, D.; Li, C.; Yang, F.; Sun, G.; You, J.; Cui, K. Synergetic effect of resins and asphaltenes on water/oil interfacial properties and emulsion stability. *Fuel* **2019**, *252*, 581−588.
(32) Liu, D.; Zhang, H.; Li, C.; Zhang, H.; Yang, F.; Sun, G.; Zhao, Y. Study on the interactive effects of solid particles and asphaltenes on the interfacial structure and stability of a water-in-model oil emulsion. *Langmuir* **2021**, *37* (36), 10827−10837.
(33) White, C. M.; Mungal, M. G. Mechanics and prediction of turbulent drag reduction with polymer additives. *Annu. Rev. Fluid. Mech.* **2008**, *40*, 235−256.

https://doi.org/10.1021/acsomega.4c08381
ACS Omega 2024, 9, 43977−43985